Gümüşhane University Journal of Science and Technology

GUFBD / *GUJS* (2016) 16(3): 840-849 doi: 10.17714/gumusfenbil.1869352 Research Article

Impact of optical filter refractive index on blue-shift effect-based multi-color visible light positioning performance

Mehmet Ali KÜÇÜK*[1], Kadir TÜRK[2]

[1]*Gümüşhane Üniversitesi, Mühendislik ve Doğa Bilimleri Fakültesi, Elektrik-Elektronik Mühendisliği Bölümü, 29100, Gümüşhane*
[2]*Karadeniz Teknik Üniversitesi, Mühendislik Fakültesi, Elektrik-Elektronik Mühendisliği Bölümü, 61080, Trabzon*

• Received: 22.01.2026 • Accepted: 12.08.2026

Abstract
The integration of visible light positioning (VLP) with multi-color visible light communication (MC-VLC) enables high-precision indoor localization without additional hardware complexity. Recent studies have shown that the blue-shift phenomenon, i.e., the angle-dependent spectral response of interference-type optical filters, can be exploited to estimate the angle of incidence (AoI). Building upon this approach, this study investigates the role of the optical filter's effective refractive index in the accuracy of blue-shift-based AoI estimation. By analyzing the eigenvalue behavior of the MC-VLC channel under different filter sets and refractive index values, it is shown that the refractive index governs the degree of nonlinearity between the eigenvalues and AoI, thereby influencing the suitability of various regression models. Simulation results demonstrate that the refractive index significantly affects positioning performance, with its impact varying across filter designs. Furthermore, numerical evaluations indicate that through appropriate filter selection, a robust and high-accuracy positioning system can be achieved even in scenarios with strong refractive-index dependence.

Keywords: Angle of arrival, Blue-shift effect, Multi-color visible light communication (MC-VLC), Optical filters, Refractive index, Visible light positioning (VLP)

1. Introduction

The integration of sensing and positioning capabilities into wireless communication networks, a paradigm known as Integrated Sensing and Communication (ISAC), has emerged as a key objective for future 6G systems (Liu et al., 2022). The widespread adoption of these converged architectures heavily relies on the development of scalable solutions that minimize hardware complexity and deployment costs. In this context, visible light positioning (VLP) has attracted considerable attention as a complementary solution to radio-frequency (RF) technologies, particularly for indoor environments (Bastiaens et al., 2024). By leveraging existing light-emitting diode (LED) infrastructures, VLP systems offer a low-cost and high-precision alternative that aligns naturally with the illumination–communication dual functionality of visible light communication (VLC) networks (Zhuang et al., 2018; Chi et al., 2020).

Conventionally, VLP systems are categorized based on their ranging techniques, with received signal strength (RSS)–based methods being widely adopted due to their simplicity (Chaudhary et al., 2021; Sun et al., 2022). These approaches rely on measuring the optical power attenuation to estimate the distance between the transmitter and the receiver, offering a solution with low computational and hardware complexity (Bastiaens et al., 2024). However, the positioning accuracy of RSS-based systems is intrinsically limited by their high sensitivity to environmental and systemic variations. In practical scenarios, fluctuations in the transmitted optical power, shadowing effects, and uncertainties in channel parameters, such as the Lambertian emission order or receiver responsivity, can introduce significant ranging errors, thereby degrading the reliability of the location estimation (Chaudhary et al., 2021). On the other hand, angle-of-arrival (AoA) techniques utilize the incidence angle of the incoming optical signal to determine the receiver's location, exhibiting improved robustness against power fluctuations compared to RSS schemes (Zhuang et al., 2018). To extract this angular information, the receiver must possess sufficient angular diversity, which typically necessitates customized hardware architectures. In the literature, various designs have been proposed to achieve this, ranging from

*Mehmet Ali KÜÇÜK; mehmetalikucuk@gumushane.edu.tr

aperture-based structures like quadrant angular diversity apertures (QADA) (Mohammed et al., 2020) and LCD-based dynamic apertures (Helderweirt & Hoeher, 2024), to orientation-based configurations where photodiodes are mounted on 3D geometrical shapes or tilted planes (Wei et al., 2016; Yang et. al., 2024). While these specialized designs significantly enhance positioning accuracy, they inevitably increase the hardware complexity and physical size of the receiver. Consequently, the reliance on bulky or non-planar structures complicates the integration with standard, compact VLC modules, limiting the practicality and widespread deployment of such solutions.

To overcome these hardware limitations, Kucuk and Turk (2026) propose leveraging the inherent angular dependence of optical filters already present in standard multi-color visible light communication (MC-VLC) receivers. This phenomenon, known as the blue-shift effect, causes the passband of interference filters to shift toward shorter wavelengths as the angle of incidence (AoI) increases (Macleod, 2017; Kucuk et al., 2024). The resulting spectral shift changes the color-channel gains, producing angle-dependent variations in the eigenvalues of the MC-VLC channel matrix. Because these eigenvalues follow a deterministic relationship with the AoI, they can be used as distinctive features for AoA estimation. Accordingly, this approach enables direct angle extraction using a conventional MC-VLC frontend, eliminating the need for specialized mechanical structures or optical components at the receiver (Kucuk & Turk, 2026).

The efficacy of this blue-shift-based positioning method is closely tied to the physical properties of the optical filters, particularly the effective refractive index. This parameter not only determines the magnitude of the spectral shift induced by changes in the angle of incidence but also governs the degree of nonlinearity in the resulting relationship between the channel eigenvalues and the AoI. As a result, variations in the refractive index directly influence the complexity of the feature mapping required for accurate angle estimation. Despite its importance, the combined effect of the refractive index on the nonlinear channel characteristics and the corresponding positioning accuracy of blue-shift-based VLP systems has received limited attention in the existing literature.

In this paper, we present a comprehensive parametric investigation of the proposed MC-VLC/P system, focusing specifically on its sensitivity to the optical filter's effective refractive index. Beyond conventional error analysis, we demonstrate that this parameter governs the degree of nonlinearity exhibited by the channel eigenvalues, thereby dictating the complexity of the AoA estimation problem. A comparative evaluation of different optical filter configurations reveals pronounced performance disparities associated with these specific hardware properties. Furthermore, we show that achieving high positioning accuracy across a wide range of refractive indices requires the joint selection of suitable filter designs and advanced nonlinear regression models. Overall, by explicitly exposing the system's parametric vulnerabilities, the findings not only provide practical design guidelines for next-generation ISAC-enabled positioning systems but also establish a critical foundation for future research aimed at mitigating these hardware-induced sensitivities.

The remainder of this paper is organized as follows. Section 2 establishes the system model and the positioning methodology, including the mathematical derivation of the blue-shift effect. Section 3 investigates the specific influence of the optical filter's refractive index on angular estimation accuracy and compares the performance of various regression techniques. Section 4 presents the comprehensive simulation results, focusing on positioning accuracy and spatial error distributions under different refractive index conditions. Finally, Section 5 concludes the paper with a summary of the findings.

2. System model and positioning method

In this section, the system model and positioning methodology evaluated in this study are presented. First, the blue-shift effect, which characterizes the angle-dependent spectral variation of optical filters, is mathematically modeled. Subsequently, the system architecture utilizing this effect as a positioning feature is detailed.

2.1. Blue-shift effect and MC-VLC channel

The fundamental mechanism enabling the proposed positioning scheme is the angular dependence of interference-type optical filters. When the incidence is non-normal, the optical path length within the multilayer structure changes, causing the spectral passband to shift toward shorter wavelengths. This phenomenon, known as the blue-shift, is directly influenced by the effective refractive index of the filter material. The angular-dependent peak wavelength, $\lambda'(\theta)$, relative to its value at normal incidence, λ_0, can be expressed as (Macleod, 2017)

$$\frac{\lambda'(\theta)}{\lambda_0} = \mu_{\mathcal{P}}(\theta) = \sqrt{1 - \frac{\sin^2\theta}{n_{\mathcal{P}}^2}}, \tag{1}$$

where θ denotes the AoI and n_P represents the effective refractive index of the optical filter for a given polarization state $\mathcal{P} \in \{s, p\}$.

To illustrate this angular dependence, Fig. 1 presents the spectral interaction between the LED power spectral density (PSD) and the shifting passband of the optical filter. The figure shows the normalized PSD of a green LED together with the lower (α) and upper (β) passband boundaries for refractive index values ranging from $n = 1.5$ to $n = 2.1$, plotted as functions of the angle of incidence.

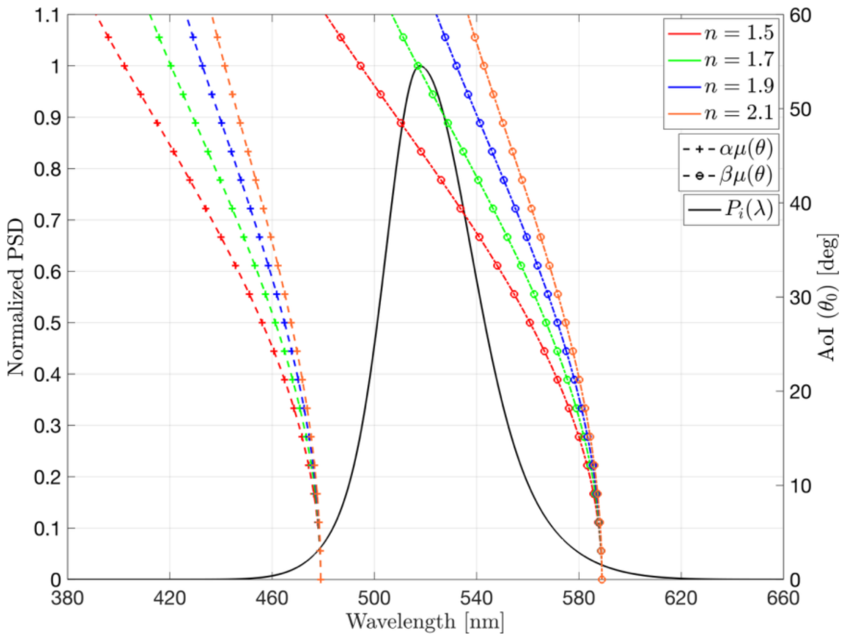

Figure 1. The variation of the optical filter passband edges (α and β) with respect to the incidence angle for different effective refractive indices and the LED PSD.

As illustrated in Fig. 1, the magnitude of the blue-shift is inversely related to the effective refractive index of the filter. Filters with lower refractive index values exhibit a more pronounced shift of their passband edges compared to those with higher index values under the same angular variation. This behavior indicates that decreasing the refractive index enhances the angular sensitivity of the filter's spectral response. Consequently, the spectral transmittance of the j-th optical filter, $\rho_j(\lambda, \theta)$, becomes explicitly dependent on the incidence angle and can be expressed as (Kucuk et al., 2024)

$$\rho_j(\lambda, \theta) = \begin{cases} T(\lambda, \theta), & \alpha\mu_{\mathcal{P}} \le \lambda < \beta\mu_{\mathcal{P}} \\ 0, & \text{otherwise,} \end{cases} \tag{2}$$

where $T(\lambda, \theta)$ denotes the peak transmittance of the passband, whose analytical formulation is given in (Kucuk et al., 2024), and $\mu_{\mathcal{P}}(\theta)$ is the polarization-dependent shift factor defined in (1).

In the context of MC-VLC, this angular spectral behavior directly influences the communication channel. The system can be represented as a multiple-input multiple-output (MIMO) channel matrix $\mathbf{H} \in R^{|D| \times |C|}$, where the DC channel gain between the i-th LED and the j-th photodetector (PD) is expressed as (Kucuk & Turk, 2026)

$$h_{ji} = \xi \int_{\lambda} P_i(\lambda)\rho_j(\lambda,\theta)d\lambda. \quad (3)$$

In this equation, $P_i(\lambda)$ denotes the PSD of the i-th colored LED. The geometric factor ξ, which contains path loss and the Lambertian emission pattern, is given by,

$$\xi = \frac{A(m+1)\cos^m(\theta)\cos(\phi)}{2\pi d^2}, \quad (4)$$

where A is the PD active area, m is the Lambertian order, d is the transmission distance, and ϕ is the irradiance angle. The integral term in (3) reveals that the channel gain h_{ji} exhibits a nonlinear dependence on the AoI due to the spectral interaction between the LED PSD and the shifted filter response $\rho_j(\lambda,\theta)$. This dependence, governed by the effective refractive index, forms the foundation for extracting angular information from the MC-VLC channel matrix.

2.2. Blue-shift effect-based positioning system

The architecture of the blue-shift effect-based MC-VLC/P system is shown in Fig. 2. Unlike conventional AoA-based positioning methods that depend on aperture-based or tilted photodiode structures, the proposed design operates entirely with standard MC-VLC receiver hardware. The positioning procedure consists of three main stages: estimation of the MC-VLC channel, prediction of the AoA using eigenvalue-based regression models, and computation of the receiver coordinates based on the estimated angles.

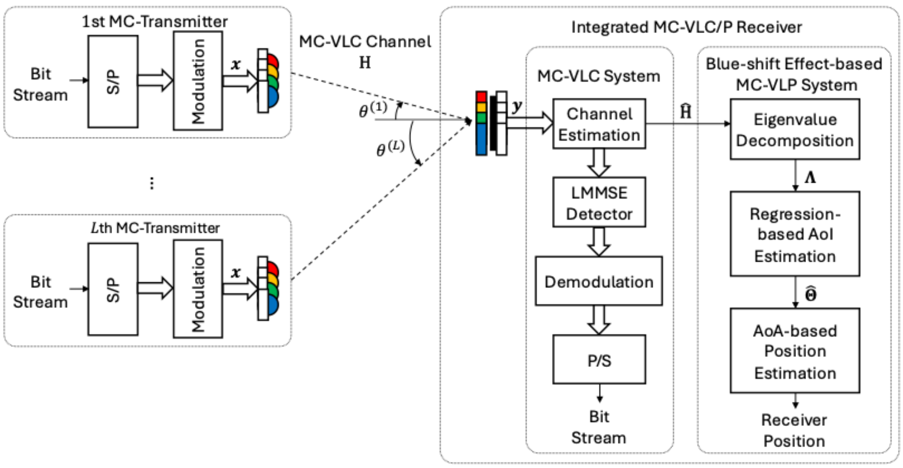

Figure 2. Block diagram of the blue-shift effect-based integrated MC-VLC/P system.

The positioning process inherently relies on accurately acquiring the channel state information. In the proposed system, the received signal can be represented as

$$\mathrm{Y} = \mathrm{HX} + \mathrm{N}, \quad (5)$$

where $\mathrm{Y} \in \mathbb{R}^{|D|\times 1}$ denotes the received signal, $\mathrm{X} \in \mathbb{R}^{|C|\times 1}$ is the transmitted signal, and $\mathrm{N} \in \mathbb{R}^{|D|\times 1}$ represents the additive white Gaussian noise (AWGN) component. To perform channel estimation, the transmitter sends a predetermined signal sequence that is known to the receiver. In alignment with the IEEE 802.15.7 standard, orthogonal sequences such as Walsh codes employed for color-shift keying (CSK) modulation are utilized for this purpose. Based on this known sequence, the estimated channel matrix, denoted as $\hat{\mathrm{H}}$, can be obtained using the conventional Least Squares (LS) method as follows

$$\hat{\mathrm{H}} = \mathrm{YX}^H(\mathrm{XX}^H)^{-1}. \quad (6)$$

After estimating the channel matrix $\hat{\mathbf{H}}$, eigenvalue decomposition (EVD) is applied to extract its eigenvalues. As shown in (Kucuk & Turk, 2026), the blue-shift effect alters the spectral integration in the channel model, leading to a nonlinear variation of the eigenvalues with respect to the incidence angle. Consequently, these eigenvalues function as distinctive features that carry the AoA information required for positioning.

Due to the complex and highly nonlinear interaction between the LED power spectral densities and the angle-dependent filter transmittance, analytically inverting the channel model to obtain the AoA is not feasible. Therefore, supervised regression methods are employed to map the extracted eigenvalues to their corresponding AoA values. In this study, linear regression, neural networks (NN), and Gaussian process regression (GPR) are evaluated for this purpose. The effective refractive index plays a key role in this mapping: it governs not only the angular sensitivity of the filter but also the degree of nonlinearity exhibited in the eigenvalue–AoI relationship. As a result, the relative performance of different regression models becomes dependent on the refractive index configuration, since each method varies in its ability to capture these nonlinear spectral interactions.

In the final stage, the estimated incidence angles ($\hat{\theta}^{(k)}$) obtained from multiple LED transmitters are used to determine the receiver's position. The horizontal distance between the receiver and each k-th transmitter is calculated as

$$r_k = \Delta z \tan\left(\hat{\theta}^{(k)}\right), \tag{7}$$

where Δz is the height difference between the transmitter and the receiver plane. This equation geometrically defines the projected 2D radial distance (r_k) on the receiver's horizontal plane based on the estimated AoI which subsequently serves as the fundamental input for the trilateration process. The 2D receiver coordinates (x, y) are then obtained by solving a non-linear least squares optimization problem that minimizes the difference between the estimated radii and the corresponding Euclidean distances as follows (Kucuk & Turk, 2026),

$$(x^*, y^*) = \arg\min_{x,y} \sum_{k=1}^{K} \left(\sqrt{(x - x_k)^2 + (y - y_k)^2} - r_k\right)^2. \tag{8}$$

This trilateration-based formulation provides robust positioning by intersecting angle estimates from at least three transmitters.

3. Impact of refractive index on angular estimation

The performance of the proposed positioning system is primarily determined by the extent to which the channel characteristics vary with the AoI. This sensitivity is directly influenced by the effective refractive index of the optical filters. To investigate this effect, we assume isotropic optical polarization behavior, i.e., $n_s = n_p = n$, and analyze the eigenvalue variations of the MC-VLC channel for different refractive index values $n \in \{1.7, 1.9, 2.1\}$. Two optical filter configurations are considered in this analysis: the Statistically Robust Design (SRD), which is optimized to suppress spectral crosstalk in multi-color systems (Ge et al., 2019), and the Full-Width at Half-Maximum (FWHM) set, a conventional design whose passbands are aligned with the spectral width of the LEDs' PSDs. At this stage of the analysis, the impact of noise is neglected to isolate the fundamental non-linear relationship between the AoI and the channel eigenvalues. This assumption allows for a evaluation of the capabilities of different regression methods to learn this non-linear mapping, without the confounding influence of noise.

Fig. 3 shows the eigenvalues of the MC-VLC channel matrix as a function of the AoI for both SRD and FWHM filter sets. The results indicate that the refractive index strongly influences the eigenvalue–AoI behavior. Lower refractive index values (e.g., $n = 1.7$) produce a more pronounced spectral shift, leading to highly nonlinear eigenvalue trajectories with steep gradients in certain angular regions. In contrast, higher refractive indices (e.g., $n = 2.1$) yield flatter and more gradually varying curves that approximate a near-linear dependence over a wider range of angles.

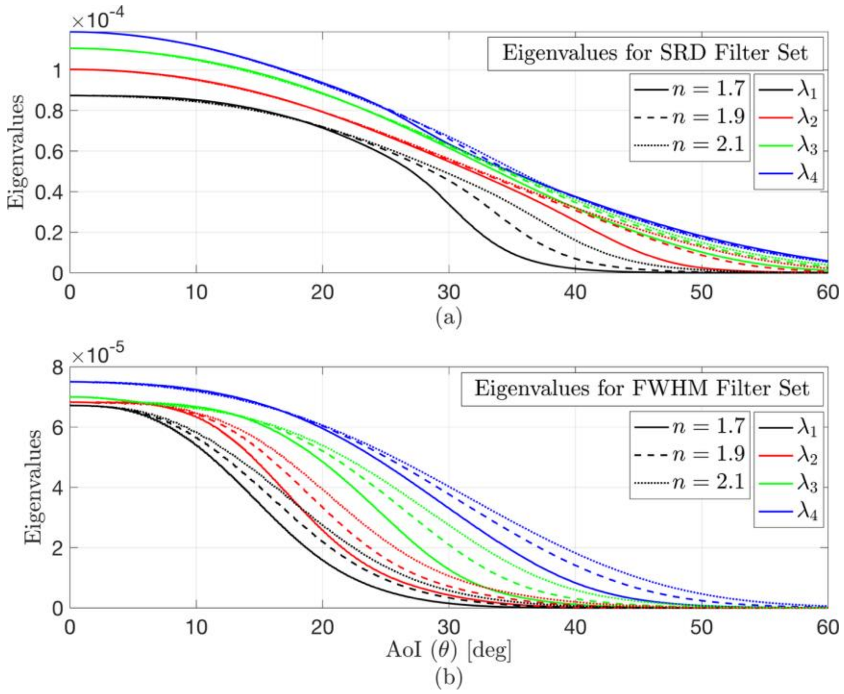

Figure 3. The variation of the channel eigenvalues with respect to the AoI for different refractive indices and different filter sets.

To quantify the AoI estimation performance of the proposed system under different filter configurations and refractive index values, three supervised regression models are evaluated: linear regression, a single-layer neural network (SL-NN) with 100 hidden neurons, and Gaussian process regression with an exponential kernel (Exp-GPR). The Root Mean Square Error (RMSE) results for these models are summarized in Table 1, providing a comparative assessment of their estimation accuracy.

Table 1. RMSE of AoI estimation for different refractive indices

		RMSE of AoI Estimation [deg]		
Filter Set	**Reg Method**	$n = 1.7$	$n = 1.9$	$n = 2.1$
SRD	Linear	1.0603	1.0008	0.8064
	SL-NN	0.0680	0.0667	0.0656
	Exp-GPR	**0.0361**	**0.0360**	**0.0363**
FWHM	Linear	2.8037	1.9239	1.3764
	SL-NN	0.2353	0.2223	0.1706
	Exp-GPR	0.0710	0.0628	0.0627

As shown in Table 1, the AoI estimation accuracy of the linear regression model improves with increasing refractive index. For example, with the FWHM filter set, the RMSE decreases from 2.80° at $n = 1.7$ to 1.37° at $n = 2.1$. This trend is consistent with the eigenvalue behavior illustrated in Fig. 3, where higher refractive indices produce flatter eigenvalue–AoI curves, thereby enabling a more linear mapping. Nevertheless, even with this improvement, linear regression performs substantially worse than the nonlinear models. Both SL-NN and Exp-GPR achieve markedly lower RMSE values across all refractive index settings by effectively capturing the underlying nonlinear spectral interaction. Therefore, only SL-NN and Exp-GPR are considered in the subsequent positioning performance evaluations.

4. Simulation setup and results

In this section, the positioning accuracy of the proposed blue-shift-based MC-VLC/P system is evaluated through numerical simulations. The effect of the optical filter's refractive index on positioning performance is examined using the cumulative distribution functions (CDFs) of the positioning error and spatial error distribution maps.

4.1. Simulation environment

A typical indoor office environment with dimensions $4 \times 4 \times 3$ m^3 is considered for the simulations. The MC-VLC system includes four multi-color LED transmitters mounted on the ceiling at predefined coordinates, and a mobile receiver positioned at a height of $z_{rx} = 0.85$ m. To perform the localization, it is assumed that the exact spatial coordinates of these LED transmitters are known a priori by the receiver. The key simulation parameters, aligned with standard MC-VLC configurations, are summarized in Table 2. Furthermore, to ensure a realistic evaluation, the shot noise and thermal noise components inherent to VLC systems are calculated and incorporated into the simulations as in (Komine & Nakagawa, 2004). In contrast to prior studies that assume a fixed refractive index, the refractive index is treated here as a variable to evaluate its effect on positioning accuracy.

Table 2. Simulation parameters

Parameter	Value
Room Dimensions	$4 \times 4 \times 3$ m^3
Tx Positions (x, y, z) [m]	$(1,1,3), (1,-1,3), (-1,1,3), (-1,-1,3)$
LED Power (P_i)	16 W
Receiver Height (z_{rx})	0.85 m
PD Area (A)	1 cm^2

4.2. Positioning accuracy analysis

To evaluate the positioning performance, 5,000 receiver locations are uniformly sampled across the room. The positioning error is defined as the Euclidean distance between the estimated coordinates (x^*, y^*) and the true receiver position. The resulting CDFs of the positioning error for different refractive indices and filter configurations are presented in Fig. 4, where subplots (a) and (b) correspond to the SRD and FWHM filter sets, respectively.

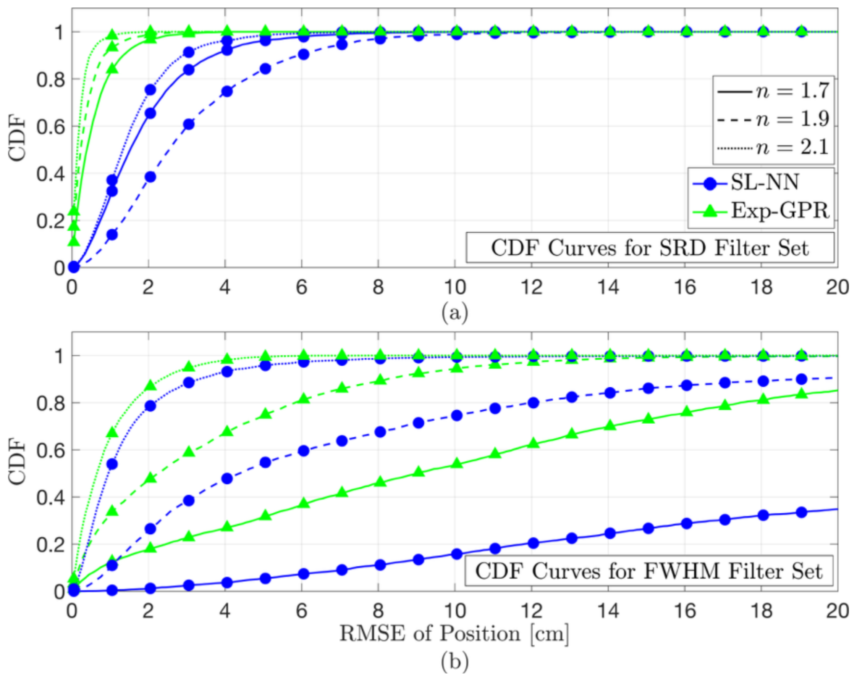

Figure 4. CDF of the positioning error for different refractive indices and filter sets: (a) SRD filter set, (b) FWHM filter set.

As shown in Fig. 4(a), the SRD filter set exhibits strong robustness to refractive index variation. The CDF curves corresponding to $n = 1.7$, $n = 1.9$, and $n = 2.1$ are closely aligned, indicating that the positioning accuracy is largely unaffected by changes in the filter material. This stability suggests that, with SRD filters, the regression models effectively capture the eigenvalue–AoI relationship over a broad range of refractive index values, enabling consistently high positioning accuracy independent of the specific filter material.

In contrast, the FWHM filter set shows a pronounced sensitivity to the refractive index, as illustrated in Fig. 4(b). While high accuracy is achieved at larger refractive indices (e.g., $n = 2.1$), a marked degradation occurs as the refractive index decreases. At $n = 1.7$, both regression models experience a substantial increase in positioning error. These results indicate that, unlike the SRD design, the performance of FWHM filters depends strongly on selecting materials with sufficiently high refractive indices.

In addition to the refractive index, channel estimation errors also significantly affect the positioning performance. These errors are directly related to the received signal-to-noise ratio (SNR). Therefore, we analyze the system performance by assuming a constant SNR value throughout the indoor environment. In this analysis, both SRD and FWHM filters are evaluated under varying SNR levels. The Exp-GPR method is exclusively used for regression, as it achieved the highest accuracy in the previous evaluations. The corresponding positioning results are presented in Fig. 5.

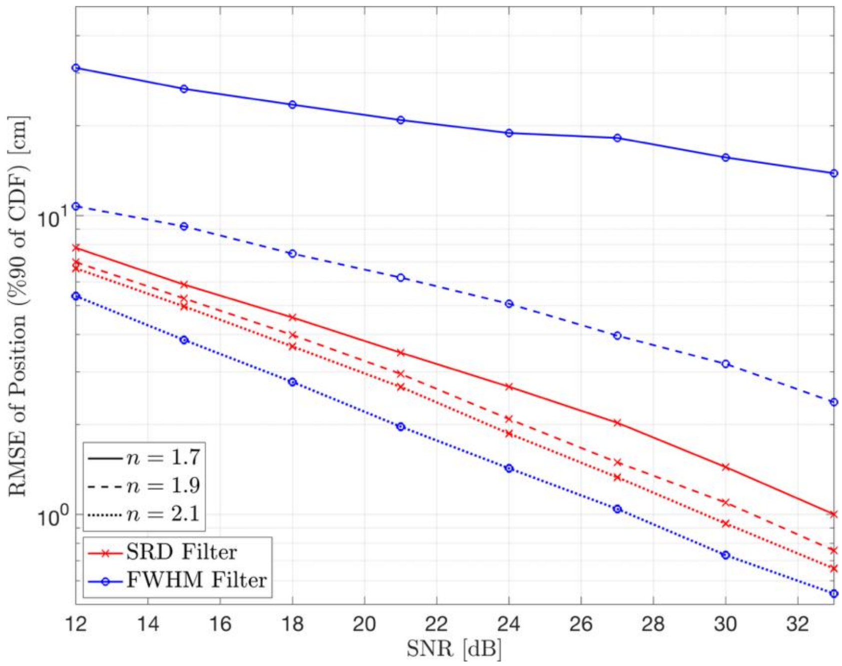

Figure 5. Positioning error as a function of SNR for the SRD and FWHM filter sets under varying effective refractive indices using the Exp-GPR method.

As can be seen in Fig. 5, increasing the SNR at the receiver reduces channel estimation errors, thereby improving the positioning performance across all filter sets and refractive index configurations. Furthermore, consistent with the previous findings, the SRD design maintains a stable and comparable performance under varying effective refractive indices. Conversely, the FWHM design exhibits a severe increase in positioning error, particularly in the low refractive index scenario.

4.3. Spatial error distribution

Finally, to provide a more comprehensive assessment of the system's reliability, the spatial distribution of the positioning error across the service area is examined. While the CDF analysis offers a global performance metric, it fails to capture location-specific degradations. Therefore, the primary objective of this section is to investigate whether the non-linear impact of the effective refractive index results in distinct spatial error patterns or non-uniform distributions within the indoor environment. Based on the CDF analysis, which highlighted the strong refractive-index dependence of the FWHM filter design, this configuration is selected for this detailed spatial evaluation.

Fig. 6 shows the spatial error maps for the FWHM filter set under two refractive index conditions: $n = 1.7$ (top) and $n = 2.1$ (bottom), obtained using the Exp-GPR method. The results reveal that changes in the refractive index primarily scale the overall error magnitude without altering the fundamental spatial structure. In both cases, the lowest errors occur near the room center, where strong line-of-sight (LoS) links ensure stable angular estimation, while the error increases toward the corners as fewer transmitters fall within the receiver's field of view. However, reducing the refractive index from $n = 2.1$ to $n = 1.7$ raises the entire error surface, indicating a uniform degradation in positioning accuracy rather than the emergence of new spatial distortions.

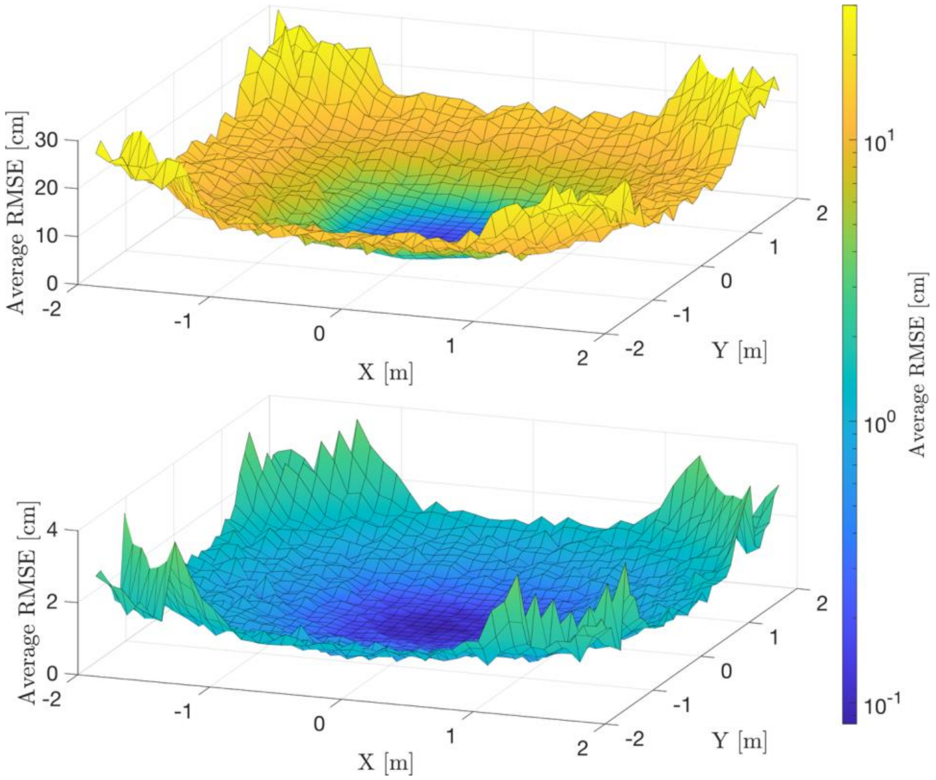

Figure 6. Spatial distribution of positioning error for $n = 1.7$ (top) and $n = 2.1$ (bottom) using FWHM filters with Exp-GPR method.

5. Conclusion

This paper investigated the influence of the effective refractive index on the performance of a blue-shift-based integrated MC-VLC/P positioning system. The results show that the refractive index plays a central role in shaping the nonlinearity between the channel eigenvalues and the AoI; lower refractive indices produce steeper spectral shifts, thereby increasing the degree of nonlinearity. A clear contrast is observed between the filter designs: the SRD filter set provides stable and index-independent performance, whereas the conventional FWHM design exhibits strong refractive-index sensitivity, with noticeable degradation at lower index values. Spatial error analysis further indicates that the refractive index primarily scales the overall error magnitude while preserving the spatial distribution pattern. These findings suggest that combining robust filter designs with nonlinear regression models offers a reliable pathway toward high-precision indoor positioning in future ISAC systems. While this study assumes stable LED spectra, developing robust AoA estimation techniques to address practical transmitter-side spectral variations, such as those induced by temperature fluctuations, remains a critical direction for future research. Furthermore, since multipath propagation can change the non-linear relationship between the channel eigenvalues and the AoI, investigating these effects is crucial for a realistic evaluation of the system's performance in practical applications.

Author contribution

Mehmet Ali Küçük: Conceptualization, Methodology, Software, Writing – original draft. Kadir Türk: Validation, Writing – review & editing, Supervision.

Declaration of ethical code

The authors of this article declare that the materials and methods used in this study do not require ethics committee approval and/or legal-special permission.

Conflicts of interest

The authors declare that there is no conflict of interest.

References

Bastiaens, S., Alijani, M., Joseph, W., & Plets, D. (2024). Visible light positioning as a next-generation indoor positioning technology: A tutorial. *IEEE Communications Surveys & Tutorials*, *26(4)*, 2867-2913. https://doi.org/10.1109/COMST.2024.3372153

Chi, N., Zhou, Y., Wei, Y., & Hu, F. (2020). Visible light communication in 6G: Advances, challenges, and prospects. *IEEE Vehicular Technology Magazine*, *15*(4), 93-102. https://doi.org/ 10.1109/MVT.2020.3017153

Chaudhary, N., Alves, L. N., & Ghassemlooy, Z. (2021). Impact of transmitter positioning and orientation uncertainty on RSS-based visible light positioning accuracy. *Sensors*, *21*(9). https://doi.org/10.3390/s21093044

Ge, P., Liang, X., Wang, J., Zhao, C., Gao, X., & Ding, Z. (2019). Optical filter designs for multi-color visible light communication. *IEEE Transactions on Communications*, *67*(3), 2173–2187. https://doi.org/10.1109/TCOMM.2018.2883422

Harlakin, A., & Hoeher, P. A. (2024). LCD-based angle-of-arrival estimation of multiple light sources: Paving the road to multiuser VLC. *IEEE Photonics Journal*, *16(3)*, 1-15. https://doi.org/10.1109/JPHOT.2024.3388928

Komine, T. & Nakagawa, M. (2004). Fundamental analysis for visible-light communication system using LED lights. *IEEE Transactions on Consumer Electronics*, *50*(1), https://doi.org/100–107. 10.1109/TCE.2004.1277847

Kucuk, M. A., Albayrak, C., Turk, K., & Yanikomeroglu, H. (2024). Optical filter design for multi-color VLC in reflective environments with multiple lighting sources. *IEEE Access*, *12*, 169344–169355. https://doi.org/10.1109/ACCESS.2024.3489792

Kucuk, M. A., & Turk, K. (2026). Blue-shift effect-based positioning for multi-color VLC. *IEEE Communications Letters*, *30*, 184-187. https://doi.org/10.1109/LCOMM.2025.3630041

Liu, A., Huang, Z., Li, M., Wan, Y., Li, W., Han, T. X., Liu, C., Du, R., Tan, D. K. P., Lu, J., Shen, Y., Colone, F., & Chetty, K. (2022). A survey on fundamental limits of integrated sensing and communication. *IEEE Communications Surveys & Tutorials*, *24*(2), 994–1034. https://doi.org/10.1109/COMST.2022.3149272

Macleod, H. A. (2017). *Thin-film optical filters* (5th ed.). CRC Press.

Mohammed, M. M. A., He, C., Cincotta, S., Neild, A., & Armstrong, J. (2020). Communication aspects of visible light positioning (VLP) systems using a quadrature angular diversity aperture (QADA) receiver. *Sensors*, *20*(7). https://doi.org/10.3390/s20071977

Sun, X., Zhuang, Y., Huai, J., Hua, L., Chen, D., Li, Y., Cao, Y., & Chen, R. (2022). RSS-based visible light positioning using nonlinear optimization. *IEEE Internet of Things Journal*, *9*(15), 14137–14150. https://doi.org/10.1109/JIOT.2022.3156616

Wei, L., Zhang, H., Yu, B., Song, J., & Guan, Y. (2016). Cubic-receiver-based indoor optical wireless location system. *IEEE Photonics Journal*, *8*(1), 1–7. https://doi.org/10.1109/JPHOT.2016.2519281

Yang, T., Zhu, B., & Zhang, Z. (2024). Over 8ksps Ultra Fast 3D Visible Light Positioning Based on Photodiodes. *2024 14th International Conference on Indoor Positioning and Indoor Navigation (IPIN)* (pp. 1-6). IEEE.

Zhuang, Y., Hua, L., Qi, L., Yang, J., Cao, P., Cao, Y., Wu, Y., Thompson, J., & Haas, H. (2018). A survey of positioning systems using visible LED lights. *IEEE Communications Surveys & Tutorials*, *20*(3), 1963–1988. https://doi.org/10.1109/COMST.2018.2806558